PCCP

PAPER

View Article Online
View Journal | View Issue

Published on 28 September 2017. Downloaded by Synchrotron Radiation Library on 05/12/2017 10:39:03.

Check for updates

Cite this: *Phys. Chem. Chem. Phys.*, 2017, **19**, 27651

Ligand displacement induced morphologies in block copolymer/quantum dot hybrids and formation of core–shell hybrid nanoobjects†

Sajan Singh,[a] Pratick Samanta,[a] Rajiv Srivastava,[a] Andriy Horechyy,[b] Uta Reuter,[b] Manfred Stamm,[bc] Hsin-Lung Chen[d] and Bhanu Nandan*[a]

Received 28th June 2017,
Accepted 28th September 2017

DOI: 10.1039/c7cp04343k

rsc.li/pccp

We investigate the self-assembly of a cylinder-forming polystyrene-*block*-poly(4-vinylpyridine) (PS-*b*-P4VP) block copolymer (BCP) mixed with trioctylphosphine oxide (TOPO) capped cadmium selenide (CdSe) quantum dots (QDs). The QDs were found to be enthalpically compatible with the P4VP chains *via* ligand displacement of TOPO from the QD surface. However, the QDs were found to localize preferentially at the PS/P4VP interphase plausibly to gain translational entropy in order to further lower the energetics of the self-assembled structure. Interestingly, the morphological transformation observed with increasing weight fraction of the QDs in the BCP/QD composite was driven by the migration of the displaced TOPO from the QD surface to the PS phase, effectively increasing its total volume fraction. Hence, the PS-*b*-P4VP BCP with PS as the minority block displayed lamellar morphology in its composite with QDs. Furthermore, the preferred localization of the QDs at the PS/P4VP interface led to the formation of a trilayer lamellar morphology which was deduced from the suppression of the primary scattering peak, relative to higher order peaks in the SAXS data. The morphological transformation was accompanied by a significant increase in the domain spacing due to excessive stretching of the longer P4VP chains of the asymmetric block copolymer. However, in the PS-*b*-P4VP/CdSe composites with P4VP as the minority block, cylindrical morphology was retained and the domain spacing decreased due to dominance of the co-surfactant effect as well as interfacial localization of CdSe QDs. We also demonstrate that these PS-*b*-P4VP/CdSe self-assembled hybrid materials could further be used to obtain isolated core–shell nanoobjects, such as nanofibers and nanosheets, containing CdSe QDs. The nanoobjects so obtained exhibited photoluminescence properties typical of CdSe quantum dots. These photoluminescent polymer nanoobjects could have potential applications in biological targeting and fluorescence labeling.

Introduction

The self-assembly of block copolymers (BCP) has been an area of intense investigation for more than two decades now. The interest in these polymers lies primarily in their ability to self-assemble into various periodic nanostructures depending on the BCP composition and block ratios.[1,2] The ordered nanoscale morphologies formed by the block copolymers and the chemically distinct nature of the blocks constituting the copolymer allow them to be used as templates to host and direct the assembly of externally added additives such as inorganic nanoparticles (NPs). Such well-ordered BCP based nanocomposites with incorporated NPs are of great interest as next generation functional materials with enhanced electronic, optical and magnetic properties. The precise control of the spatial organization of the NPs is one of the crucial factors which affects the ultimate performance of these hybrid materials. Hence, a number of studies, both theoretical and experimental, have been carried out in this direction, with a focus on controlled localization of nanoparticles in the microphase separated structure of block copolymers.[3–11]

The past studies have shown that the localization of NPs in a block copolymer is thermodynamically governed by a delicate interplay between the entropic and enthalpic contributions.[3,8,12,13]

[a] *Department of Textile Technology, Indian Institute of Technology Delhi, Hauz Khas, New Delhi 110016, India. E-mail: nandan@textile.iitd.ac.in*
[b] *Leibniz Institute of Polymer Research Dresden, Hohe Strasse 6, Dresden 01069, Germany*
[c] *Technische Universität Dresden, Physical Chemistry of Polymer Materials, Dresden 01062, Germany*
[d] *Department of Chemical Engineering, National Tsing-Hua University, Hsinchu 30013, Taiwan*

† Electronic supplementary information (ESI) available: Composition details of the samples; TEM micrographs of neat $S_{178}VP_{386}$ block copolymer showing bulk morphology and nano-object structures; ^{31}P NMR of the block copolymer/CdSe composite; TGA plot of TOPO-coated CdSe; UV-vis and PL spectra of block copolymer/CdSe composites in chloroform. See DOI: 10.1039/c7cp04343k

Published on 28 September 2017. Downloaded by Synchrotron Radiation Library on 05/12/2017 10:39:03.

The enthalpic contribution is mainly dictated *via* the selective or non-selective interaction of the nanoparticles with the monomer units of the polymer chains, whereas the entropic contribution arises from the stretching of the polymer chains (conformational entropy) to accommodate the NPs. Apart from this the translational entropy of nanoparticles within the self-assembled structure formed by the block copolymer also influences their localization. The previous studies carried out on BCP/NP composites have revealed that if the NPs are strongly selective towards one of the blocks, the enthalpic contribution dominates such that the NPs are localized uniformly in the domain formed by the interacting block.[12] Furthermore, if the NPs are completely neutral towards both the blocks then they tend to distribute at the interface formed by the two blocks. However, when the nanoparticles only weakly interact with one of the blocks, the situation becomes much more complex and the entropic contributions also become significant in the final morphology. The theoretical work carried out by Balazs and coworkers has shown that if the particles are chemically identical to one of the blocks (weak enthalpic interactions), the size of the NPs becomes crucial in governing their localization in the self-assembled domains.[14–22] It was shown that large NPs ($d/L \sim 0.3$, where d is the NP diameter and L is the lamellae domain width) concentrated in the center of the preferred domain in order to minimize the entropic penalty associated with stretching of the polymer chains in this domain.[15,16] Smaller NPs ($d/L < 0.2$) were shown to be concentrated nearer to the BCP domain interface so as to maximize the translational entropy associated with the NPs. Moreover, if the particle sizes are comparable to the radius of gyration of the block, macrophase separation of the particles occurs that may co-exist with a fairly disordered block copolymer morphology. Furthermore, the theoretical work of Balazs and co-workers has also demonstrated that apart from the particle size and chemistry, the morphology of BCP/NP composites is also influenced by the shape of the particles.[20]

These theoretical findings have been corroborated by a number of experimental studies carried out on BCP/NP composites in the past few years. Bockstaller *et al.* demonstrated that the size of nanoparticles stabilized with aliphatic ligands dictated their localization in the domains formed by the polystyrene-*block*-poly(ethylene-propylene) (PS-*b*-PEP) copolymer.[23] Hence, gold (Au) NPs with $d/L \sim 0.06$ segregated to the interface whereas the large silica NPs with $d/L \sim 0.26$ almost exclusively localized in the center of PEP domains. Chiu *et al.* also made a similar but more systematic study in which PS capped Au nanoparticles were incorporated into symmetric PS-*b*-P2VP.[24] Kramer and coworkers demonstrated that the location of Au NPs in the PS-*b*-P2VP could be tuned by judicious functionalization of the NPs with thiol terminated PS and P2VP oligomers.[25] Hence, Au NPs functionalized with PS or P2VP chains were found to localize within the PS or P2VP domains whereas those having both PS and P2VP chains at the surface were found to locate at the interface. The same group further demonstrated that the location of PS modified Au NPs in the self-assembled domains of the PS-*b*-P2VP copolymer could also be tuned by varying the areal chain density of the PS ligands.[26–28] When the NPs were completely shielded by the PS chains they tend to localize in the PS domains. However, the partially shielded Au NPs were found to locate along the interface because of the preferential interaction of the AuNPs with the P2VP chains. Furthermore, the increased loading of NPs in block copolymers was also shown to induce order–order and order–disorder transitions in the self-assembled morphologies.[29–34] Gai *et al.* have shown that by manipulating strong enthalpic interactions between the NPs and one of the blocks, very high loading of NPs could be achieved selectively in one of the domains without any morphological transformation.[35] Moreover, the same approach could also be used to localize large NPs selectively in one of the domains which otherwise would undergo macrophase separation.[36] It must be noted that in all the above-mentioned studies, the ligand was strongly bound to the NPs and remained attached to the NP surface in the BCP/NP composites.

The microphase separated BCP/NP composites in bulk further provide possibilities to fabricate nanoparticle loaded functional polymer nano-objects by selectively swelling the matrix phase of the self-assembled structures and isolating the nanoparticle containing domains.[37] Zhu and coworkers incorporated PS stabilized gold (Au) nanoparticles in the PS cylindrical or spherical domains of supramolecular assembly composed of PS-*b*-P4VP and pentadecylphenol (PDP).[38–40] It was shown that by selectively dissolving the PDP present in the P4VP(PDP) matrix phase, polymer nanofibers and nanospheres loaded with Au nanoparticles in the core could be isolated. The location of the nanoparticles was also shifted from the PS core of the nanoobjects to the interface by tuning the ligand chemistry of the Au nanoparticles. Recently, we demonstrated an even simpler approach for obtaining cylindrical micellar aggregates or nanofibers with encapsulated nanoparticles.[41–43] It was shown that the PS stabilized silver (Ag) nanoparticles were incorporated in the PS cylindrical domains of a PS-*b*-P4VP block copolymer which then could be further isolated as nanofibers by dispersing the bulk self-assembled structure in a P4VP selective solvent. The Ag nanoparticles in this case were packed in a helical symmetry in the core of the nanofiber which demonstrated that a range of interesting possibilities exists with this approach.[43]

In the present work, the self-assembly behavior of PS-*b*-P4VP diblock copolymers mixed with TOPO stabilized CdSe quantum dots (QDs) has been investigated. It will be demonstrated that the morphology of the PS-*b*-P4VP/CdSe composites was strongly influenced by the displacement and subsequent migration of the TOPO ligands preferably towards the PS phase. Furthermore, it will also be shown that the self-assembled morphologies of the PS-*b*-P4VP/CdSe composites could be used to fabricate CdSe functionalized polymer nanostructures such as nanofibers and nanosheets. The isolated nanostructures depicted fairly good fluorescence properties typical of CdSe QDs.

Experimental

Materials

Polystyrene-*block*-poly(4-vinylpyridine) of two different molecular weights *i.e.* $PS_{18.5K}$-*b*-$P4VP_{40.5K}$ (M_w/M_n = 1.10) and $PS_{56.5K}$-*b*-$P4VP_{22.5K}$ (M_w/M_n = 1.09) were purchased from Polymer

 This journal is © the Owner Societies 2017

Published on 28 September 2017. Downloaded by Synchrotron Radiation Library on 05/12/2017 10:39:03.

source, Canada. The $PS_{18.5K}$-*b*-$P4VP_{40.5K}$ and $PS_{56.5K}$-*b*-$P4VP_{22.5K}$, hereafter, will be referred to as $S_{178}4VP_{386}$ and $S_{543}4VP_{214}$, respectively, where the subscript in the sample codes refers to the degree of polymerization of the respective blocks. Cadmium oxide (CdO, 99.5%), trioctylphosphine oxide (TOPO, 99%), trioctylphosphine (TOP, 99%), 1-octadecene (ODE, 90%), oleic acid (OA, 90%), and selenium powder mesh (99.99%) were purchased from Sigma-Aldrich. Octadecylamine (ODA, 97%) was purchased from Merck Chemicals. All the solvents used were anhydrous and were purchased from Merck chemicals.

Synthesis of CdSe quantum dots

CdSe QDs were synthesized as reported elsewhere.[44] 0.1 mmol of Se was dissolved in 3.5 mL of TOP at room temperature in a glove box. 10 mL of 1-octadecene was mixed with 0.1 mmol of CdO and 0.4 mmol of oleic acid in a 4 necked round bottom flask and heated to 280 °C with continuous stirring until a clear solution was obtained. Subsequently the temperature was lowered to 80 °C after which 3 g of ODA and 2 g of TOPO were added to the solution. The solution was then heated to 280 °C under continuous stirring. Later, the solution of already prepared TOP–Se was injected into the hot Cd solution. The temperature of the solution was then lowered to 260 °C. The reaction was allowed to proceed until the desired size of nanoparticles was obtained. The nanoparticles were purified by phase separation using a 1 : 1 (v/v) mixture of hexane–methanol, precipitated by acetone and finally re-dispersed in chloroform. The concentration of the nanoparticles was determined by UV-vis absorption spectroscopy.

Preparation of BCP/CdSe composites and nanoobjects

The PS-*b*-P4VP block copolymer was dissolved in chloroform, which is a common solvent for both PS and P4VP, at room temperature and then CdSe QDs dispersed in chloroform were added dropwise to the block copolymer solution under continuous stirring. The solution was kept under continuous stirring for 48 hours. The BCP/CdSe composite solution was then kept in a saturated vapour atmosphere of chloroform in a closed chamber with a very small opening for slow solvent evaporation. After complete evaporation of the chloroform, the sample was kept in a vacuum oven for 48 h at room temperature to remove the traces of solvent present. The bulk samples so obtained were re-dispersed in ethanol or cyclohexane to isolate the CdSe containing polymer nanoobjects from the self-assembled morphologies of BCP/CdSe composites.

Characterization

SAXS measurements were conducted at beamline BL23A1 of the National Synchrotron Radiation Research Center (NSRRC), Hsinchu, Taiwan.[45] The energy of the employed monochromatic radiation was 15 keV, corresponding to a wavelength of 0.83 Å. The 2D scattering patterns were collected with a Mar charge-coupled device (CCD) detector. The measured scattering wave vector q ranged from 0.07 to 4.0 nm^{-1} ($q = 4\pi \sin(\theta)/\lambda$, where 2θ is the scattering angle and λ is the wavelength). Samples were held in the Kapton cells with the exposure time of 60 s. The collected scattering patterns were radially averaged to obtain one-dimensional (1D) scattering intensity profiles. All the scattering profiles were corrected for scatterings from the air and cell. Transmission Electron Microscopy (TEM) was performed using a JEOL JEM-2100F transmission electron microscope at an accelerating voltage of 200 kV. The bulk samples for TEM imaging were prepared by ultramicrotoming and placed onto carbon coated copper grids. The specimens for TEM imaging of the isolated nano-objects were prepared by drop casting the BCP/CdSe composite dispersion in a selective solvent onto a carbon coated copper grid. UV-vis absorption spectra were recorded on a Perkin-Elmer Lambda 1050 spectrophotometer. Dilute solutions of QDs in chloroform and nanoobjects in methanol or cyclohexane were placed in four window 1 cm quartz cuvettes, and their absorption and corresponding fluorescence were measured. The fluorescence spectra were acquired on a Perkin-Elmer LS-55 spectrometer with constant 10 nm excitation and emission slit width with an excitation wavelength of 344 nm. ^{31}P NMR was carried out using a Bruker-300 NMR instrument operating at 300 MHz using trioctylphosphine as an internal standard.

Results and discussion

The PS-*b*-P4VP block copolymers of two different molecular weights were so chosen such that one was expected to form PS cylinders embedded in a P4VP matrix ($S_{178}VP_{386}$) whereas the other was expected to form P4VP cylinders embedded in a PS matrix ($S_{543}VP_{214}$). The neat block copolymers were first characterized to ascertain their self-assembled structures. Fig. 1 shows the SAXS intensity curves of the two different PS-*b*-P4VP block copolymers used in this work.

The SAXS intensity profile of the neat $S_{178}VP_{386}$ block copolymer shows a strong primary peak at $q \sim 0.13$ nm^{-1} and a broad hump at higher q. The TEM result revealed that this copolymer formed PS cylinder morphology but the arrangement of the cylindrical domains was not ordered enough to yield clear higher-order diffraction peaks in the SAXS profile (please see the ESI†). The SAXS intensity profile of the neat $S_{543}VP_{214}$ block copolymer displayed a strong primary peak

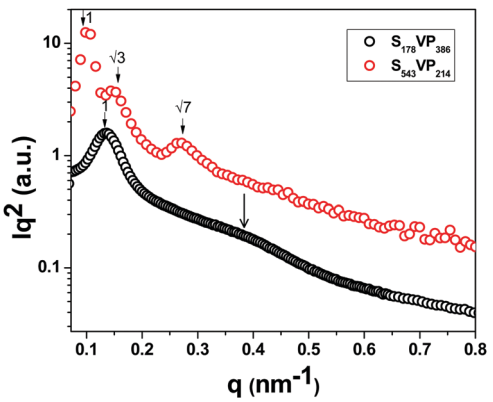

Fig. 1 SAXS intensity profiles of neat block copolymers used in the study.

Published on 28 September 2017. Downloaded by Synchrotron Radiation Library on 05/12/2017 10:39:03.

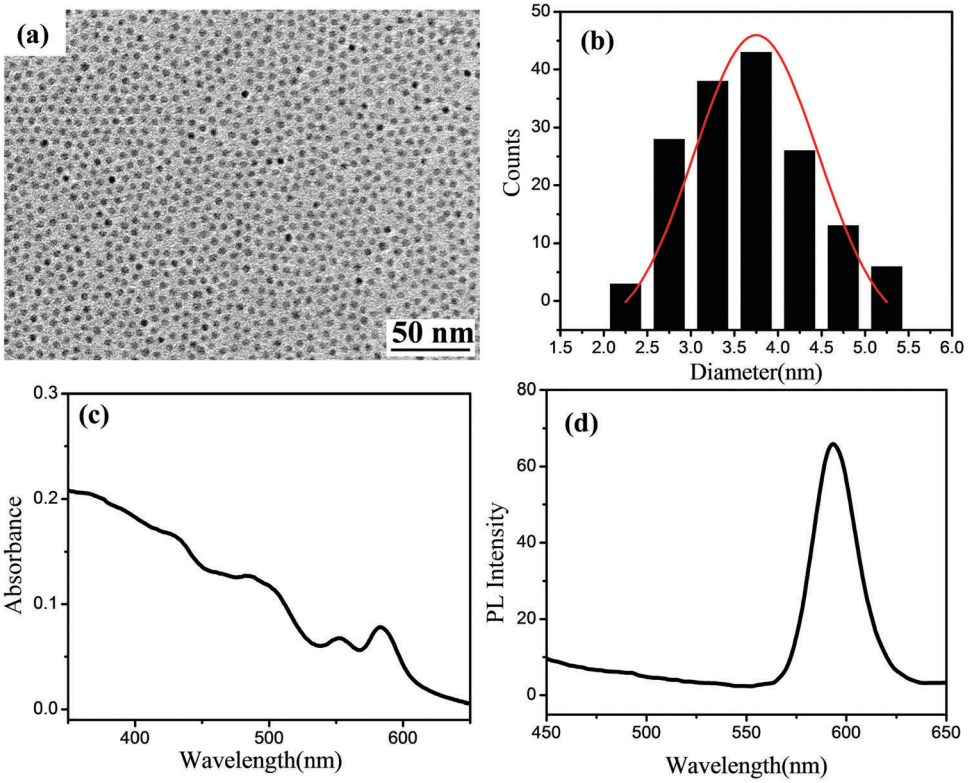

Fig. 2 (a) TEM image, (b) corresponding size histogram, (c) UV-vis absorption and (d) photoluminescence spectra of TOPO capped CdSe quantum dots.

situated at $q \sim 0.10\ \mathrm{nm}^{-1}$ and higher-order peaks. The ratio of the peak positions followed $1:\sqrt{3}:\sqrt{7}$, suggesting that the self-assembled cylindrical domains formed by the minority P4VP blocks were hexagonally packed. The hexagonal packing of cylinders is known to result in SAXS peaks in the ratio $1:\sqrt{3}:\sqrt{4}:\sqrt{7}:\sqrt{9}:\sqrt{12}$. Next, the CdSe quantum dots were synthesized and characterized. Fig. 2(a) and (b) shows the HRTEM images of the as-synthesized CdSe QDs and the corresponding size distribution plot of the diameters obtained. The figure shows that the QDs were fairly uniform in size and had an average diameter of 3.8 nm.

Furthermore, the as-synthesized QDs exhibited typical UV-vis absorption and emission properties as shown in Fig. 2(c) and (d), respectively. The first excitonic peak was observed at 583 nm in the absorption spectra and the corresponding emission peak at 593 nm in the emission spectra. Next, we proceed to discuss the bulk morphology of the PS-*b*-P4VP/CdSe composites.

Bulk morphology of $S_{178}VP_{386}$/CdSe composites

The bulk morphologies of the $S_{178}VP_{386}$/CdSe composites were ascertained using a combination of SAXS and TEM measurements. Fig. 3 shows the SAXS intensity profile of $S_{178}VP_{386}$/CdSe composite samples. The loading of CdSe NPs in the composites was varied from 0 to 50 wt%.

In the low-q region of the SAXS profiles shown in Fig. 3(a), at 10 wt% of CdSe NPs in the composites, a primary scattering peak and several higher order peaks were observed. Interestingly, the positions of the higher-order peaks were found to be integer multiples of the first-order peak, suggesting the formation of alternating lamellar domains with a long range spatial order. As discussed previously, the neat BCP exhibited PS cylinder morphology, as was expected from the volume fraction of the PS (f_{PS}) present in the BCP. Hence, the SAXS results revealed that a phase transition from cylinder to lamellar morphology occurred at even the lowest content of added CdSe QDs to the block copolymer, *i.e.* 10 wt%. The amount of quantum dots incorporated in block copolymers affects the polymer conformational entropy and particle translational entropy apart from the system enthalpy. Hence, the concentration of quantum dots can indeed result in order–order or order–disorder transition because of its resultant influence on interfacial curvature. Such morphological transitions, in the past, have been observed for a number of block copolymer/nanoparticle mixtures.[3,12] However, in most of the cases, the morphological transitions have been reported at much higher weight/volume fractions of nanoparticles in the block copolymer. Yeh *et al.* showed that in the case of PS-*b*-P4VP/CdS composites, order–order phase transition from hexagonally packed P4VP cylinders in neat BCP to lamellar morphology occurred at a much lower weight fraction of CdS nanoparticles (*ca.* 7.5 wt%).[31] It was postulated that the dipole–dipole interaction between the ligand surrounding the CdS nanoparticles and pyridine units restricted the mobility of P4VP chains which possibly induced the phase transition. The results were also explained using the theoretical phase diagram proposed by Balazs and coworkers for block copolymer/nanoparticle mixtures. However, the theoretical

 This journal is © the Owner Societies 2017

Published on 28 September 2017. Downloaded by Synchrotron Radiation Library on 05/12/2017 10:39:03.

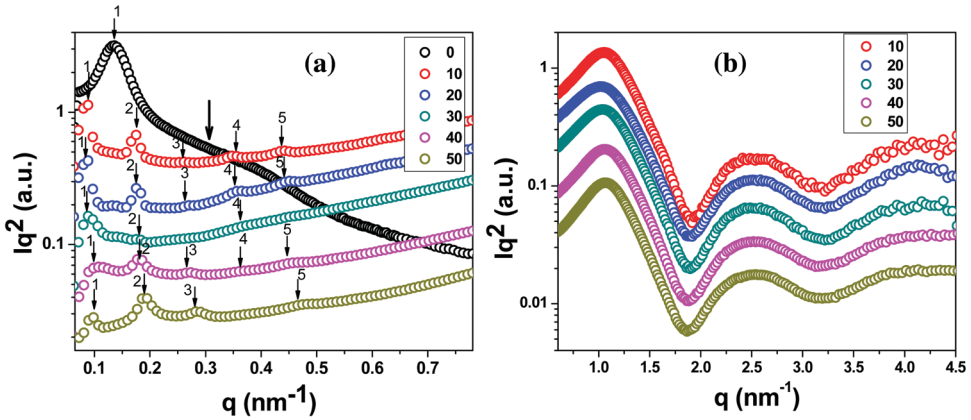

Fig. 3 SAXS intensity profiles of $S_{178}VP_{386}$/CdSe composites, at different loadings of CdSe QDs (wt%), in the (a) low-q and (b) high-q region.

phase diagram corresponded to a much higher volume fraction of nanoparticles (*ca.* 0.15) in the block copolymer.[18]

The morphological transformation observed for the $S_{178}VP_{386}$/CdSe composites in the present study could be understood by first investigating the localization of the CdSe quantum dots in the self-assembled PS-*b*-P4VP block copolymer morphologies. The CdSe quantum dots used in this work were stabilized by a layer of surface ligands of octadecylamine, trioctylphosphine and trioctylphosphine oxide, which is being collectively referred to as TOPO here. It has been shown in the past that pyridine groups are effective at displacing TOPO from the surface of CdSe quantum dots and, hence, P4VP effectively could serve as a multidentate ligand for the quantum dots.[46–49] This was corroborated by ^{31}P NMR measurements of the PS-*b*-P4VP/CdSe mixture in $CDCl_3$. The ^{31}P NMR of the PS-*b*-P4VP/CdSe mixtures displayed a sharp signal at 48 ppm (please see the ESI†), which corresponded to free TOPO ligands in $CDCl_3$.[47,48,50] This explicitly showed that ligand displacement occurred in the presence of P4VP. Hence, the CdSe quantum dots were expected to localize in the P4VP domains of the PS-*b*-P4VP self-assembled morphologies. As will be shown later using TEM analysis, the CdSe quantum dots were indeed found to locate in the P4VP domain although there was a preference for the particles to localize closer to the interface. However, such a scenario was expected to increase the total volume fraction of the P4VP matrix phase of a $S_{178}VP_{386}$ block copolymer which meant that either the cylindrical morphology should have been preserved or a morphological transformation to spherical morphology should have been the case. The fact that the lamellar morphology was formed even at 10 wt% of CdSe quantum dots indicated that the addition of nanoparticles somehow increased the total PS volume fraction. It is plausible that the TOPO ligands which were displaced by the P4VP chains from the surface of CdSe quantum dots migrated to the PS phase. This was expected as a result of the favorable hydrophobic molecular interactions between TOPO and PS chains. Zou *et al.* have shown that in thin films of PS-*b*-P2VP mixed with TOPO bound CdSe quantum dots, the CdSe quantum dots were preferentially located in the PS domains because of the favorable interaction between TOPO and PS.[51] Interestingly, it has been found that because of steric restrictions in the accessibility of the nitrogen atom, P2VP has much weaker interactions with the CdSe quantum dots as compared to P4VP.[46] Now, from thermogravimetric analysis it was found that TOPO constituted nearly 42 wt% of the TOPO coated CdSe quantum dots (please see the ESI†). Moreover, in terms of volume fraction, the TOPO volume fraction was much higher because of the lower density of TOPO as compared to CdSe. Hence, assuming that most of the TOPO displaced from the CdSe quantum dots migrated to the PS phase, the net effect of this in increasing the volume fraction of the PS phase was expected to be much higher than those of CdSe quantum dots expected to be in the P4VP phase. For instance, at a 10 wt% loading of quantum dots in $S_{178}VP_{386}$, the volume fraction of the PS domain was 0.364, whereas that of P4VP(CdSe) was found to be 0.636, assuming that all the TOPO has migrated to the PS phase. Such a shift in the effective composition of the PS phase clearly explains the observed morphological transition to a lamellae phase. The volume fraction of TOPO at 10 wt% loading of CdSe QDs was $\sim$0.051 which could be considered as the threshold amount of TOPO migration required for the cylinder to lamellae transition in the present system.

The lamellar morphology of the $S_{178}VP_{386}$/CdSe composites was further corroborated from the real-space morphological analysis carried out using TEM measurements. Fig. 4 shows the TEM images of the microtomed specimens obtained from bulk $S_{178}VP_{386}$/CdSe composite samples.

The TEM image, at 10 wt% of CdSe quantum dots, clearly revealed the lamellar morphology of the composites. However, a few circular domains were also observed in the TEM image which plausibly suggested that a small fraction of kinetically trapped cylindrical microdomains was retained in this sample. The P4VP layer appeared relatively dark because of its slight higher electron density in comparison to the PS phase. Furthermore, the CdSe quantum dots were mostly found to locate within the P4VP layer. However, the density of quantum dots was observed to be higher towards the interface. This plausibly was because of the relatively small size of the quantum dots such that interface localization allowed the particles to have maximum translational entropy. Furthermore, it is also possible that a fraction of the TOPO ligands remain bound to the CdSe QDs such that they impart partial hydrophobic character to the

Published on 28 September 2017. Downloaded by Synchrotron Radiation Library on 05/12/2017 10:39:03.

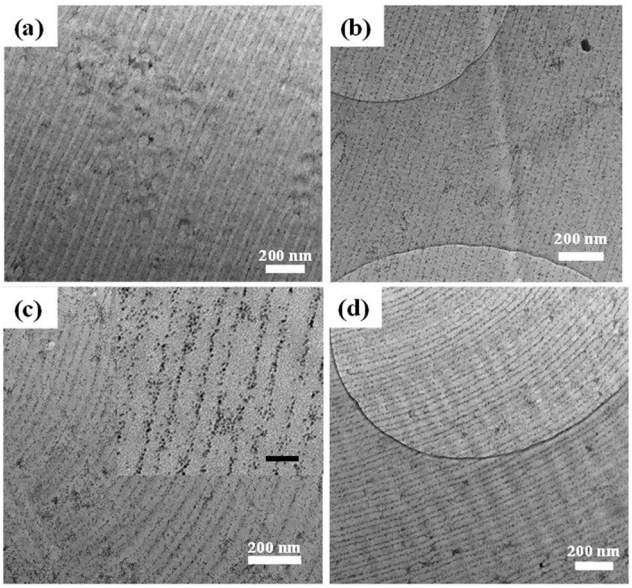

Fig. 4 TEM images of $S_{178}VP_{386}$/CdSe composites at different CdSe loadings (wt%): (a) 10, (b) 30, (c) 40, (d) 50. The inset in (c) shows a higher magnification image where the scale bar corresponds to 50 nm.

QDs. Such a scenario is also likely to drive the migration of QDs closer to the interface.

At a higher loading of CdSe quantum dots, the lamellar morphology was retained as ascertained from the SAXS data shown in Fig. 3(a) as well as the TEM images shown in Fig. 4. In all cases, the ratio of the position of the higher order peaks with respect to that of the primary scattering peak was found to be 1 : 2 : 3 : 4. Interestingly, as the weight fraction of the quantum dots in the block copolymer increases, the intensity of the primary scattering peak with respect to the higher order peak was found to decrease. This was much more prominent in the samples with 40 and 50 wt% CdSe quantum dots where the intensity of the primary scattering peak was much lower than the second order peak. The disappearance of the first order peak for a lamellar morphology has been reported in the past for systems displaying a tri-layered structure such as three-layer lamella in triblock copolymers.[52–54] It has been shown that the disappearance of the first order scattering peak for a triblock lamellar system could be due to the scattering from the following two cases: one is that there are at least three different self-organized lamellar layers with the electron density of the middle layer either higher or lower than that of the two neighboring layers; and the other is from three self-organized lamellae with one layer's electron density apparently larger than the others. In the present study where a diblock was used, the reduced intensity of the first order peak was intriguing. However, the scattering results could be clearly explained from the TEM images of the corresponding sample morphologies as shown in Fig. 4. It was observed that a lamellar morphology was preserved for all $S_{178}VP_{386}$/CdSe compositions studied. Most interestingly, as the weight fraction of CdSe quantum dots was increased in the composites, the density of quantum dots localized at the lamellar interface also increased. At 40 and 50 wt% CdSe quantum dots, three distinct layers in the lamellar morphology could be clearly observed which included two layers constituted mostly of the PS and P4VP block whereas the third and middle layer was formed because of the accumulation of the CdSe quantum dots at the interface. The morphology was identical to that observed for triblock copolymers displaying lamellar morphologies. The much higher electron density of the middle layer composed of predominantly CdSe quantum dots compared to the layer composed mostly of PS and P4VP blocks led to the observed diminished intensity of the first order peak.

Fig. 5 shows the variation of the domain spacing with CdSe concentration in the composite, as ascertained from the primary peak position of the SAXS data (peak positions, q, were converted to domain spacing, d, using the relation: $d = 2\pi/q$). It was interesting to note that the domain spacing increased significantly upon addition of 10 wt% CdSe quantum dots in the block copolymer. Furthermore, at a higher loading of CdSe quantum dots a small reduction in the domain spacing was observed.

The significant increase in the domain spacing on morphological transformation from cylinder to lamellae, upon addition of CdSe quantum dots, could be explained from the schematic illustration depicted in Fig. 6.

The neat $S_{178}VP_{386}$ block copolymer displayed morphology where the hexagonally packed cylinders of PS were embedded in the P4VP matrix. The interfacial curvature allowed the longer P4VP blocks to relax so as to gain conformational entropy. However, in the $S_{178}VP_{386}$/CdSe composites, the morphology transformed to a lamellar structure due to migration of TOPO to the PS phase. In the lamellar morphology, the relaxed conformation of longer P4VP blocks, similar to that in the cylindrical case, is likely to result in a significant increase in the interfacial energy. This necessitated the P4VP chain to stretch normal to the lamellar interface so as to minimize the increase in the interfacial energy. This argument is also corroborated from the fact that once the morphology was transformed to lamellar at 10 wt% CdSe quantum dots, further increase in the CdSe concentration in the composite did not lead to additional increase in the interdomain spacing. The loss in conformational

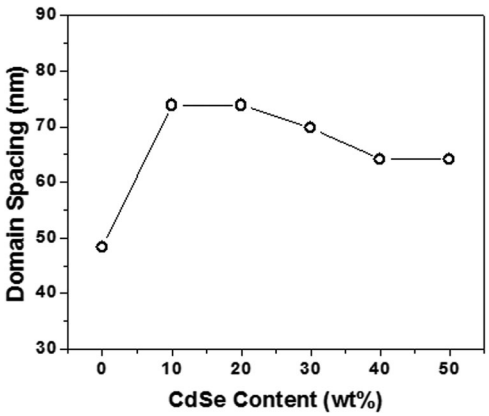

Fig. 5 Domain spacing variation with CdSe content for $S_{178}VP_{386}$/CdSe composites.

 This journal is © the Owner Societies 2017

Published on 28 September 2017. Downloaded by Synchrotron Radiation Library on 05/12/2017 10:39:03.

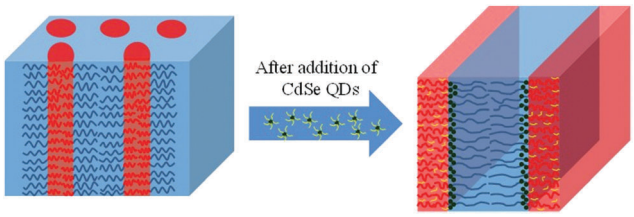

Fig. 6 Schematic illustration depicting the cylinder to lamellae transition upon addition of TOPO coated CdSe quantum dots in $S_{178}VP_{386}$/CdSe composites. The stretching of longer P4VP chains in the lamellar morphology led to a significant increase in domain spacing.

entropy in this case was plausibly compensated due to the favorable enthalpic interactions between PS and TOPO. The behavior is similar to the observed increase in the interdomain spacing of block copolymers in the presence of a selective solvent.[55,56] A very small decrease in the interdomain spacing observed at a very high loading of CdSe quantum dots is not clear to us at present. However, this plausibly could be due to the significant accumulation of the nanoparticles/TOPO at the interface thereby reducing the interfacial tension between the PS and P4VP phases. Apart from this, it should also be noted that the crowding of the CdSe nanoparticles at the interface may lead to increase in the interfacial area per chain. In such a scenario, the PS and P4VP chains will contract for volume filling requirements. This could also contribute to the reduction in the domain spacing. Furthermore, another factor which may also contribute to the reduction in the domain spacing is that TOPO migrating to the PS domain was expected to wet the PS chains. This will also result in increase in the interfacial area per chain where the PS chains will stretch but the P4VP chains will contract.[57–60]

The high-q scattering profile of the $S_{178}VP_{386}$/CdSe composites is shown in Fig. 3(b). All the scattering profiles showed a very intense peak at $q \sim 1.00$ nm^{-1} and two broad peaks at $q \sim 2.6$ and 4.1 nm^{-1}. It is proposed that the peak at $q \sim 1.00$ nm^{-1} originated due to scattering from closely packed quantum dots and corresponded to an average spacing between the particles. Furthermore, the broad peaks in the high-q region, at $q \sim 2.6$ and 4.1 nm^{-1}, resulted from the intraparticle scattering from the individual nanoparticles. The scattering profile was fitted in the high-q region using a sphere form factor which provided the average diameter of the CdSe quantum dots to be ~4.2 nm. The diameter was close to that found using HRTEM and UV-vis spectroscopy results.

Bulk morphology of $S_{543}4VP_{214}$/CdSe composites

The bulk morphologies of the $S_{543}VP_{214}$/CdSe composites were also ascertained using a combination of SAXS and TEM measurements. Fig. 7 shows the SAXS intensity profile of $S_{543}VP_{214}$/CdSe composite samples. The loading of CdSe NPs in the composites was varied from 10 to 60 weight percent. In the low-q region of the SAXS profiles shown in Fig. 7(a), between 10 and 40 wt% of CdSe NPs in the composites, a primary scattering peak and a few higher order peaks were observed. The primary and higher order peak positions corresponded to a ratio of $1:\sqrt{4}:\sqrt{7}:\sqrt{12}$ which revealed hexagonally packed cylindrical morphology of the $S_{543}VP_{214}$/CdSe composite samples. It must be noted that the neat $S_{543}VP_{214}$ block copolymer also displayed similar morphology as already discussed. Hence, in this case, the cylindrical domain morphology of the block copolymer was preserved unlike for the $S_{178}VP_{386}$/CdSe composites where the morphology transformed to lamellae.

In the $S_{543}VP_{214}$ block copolymer, the PS constituted the majority block. Hence, the migration of TOPO to the PS phase retained the asymmetric composition of the block copolymer and the composition shifted more towards the spherical morphology as the weight fraction of CdSe in the blend increases. Furthermore, since the TOPO migrated to the majority PS phase, the changes in the volume fraction of the different phases were also not as pronounced as for the case of $S_{178}VP_{386}$/CdSe composites. At further higher weight fraction of the CdSe quantum dots in the composite (*i.e.* ≥50 wt%), the SAXS profile displayed only a strong primary scattering peak and another broad higher order peak. The scattering profile was typical for a microphase separated structure of block copolymer without any long range order. In this case, the primary scattering peak corresponded to the average distance between the microphase separated domains and the higher order peaks originated from the scattering due to the individual domains. The SAXS data in the high-q region, shown in Fig. 7(b),

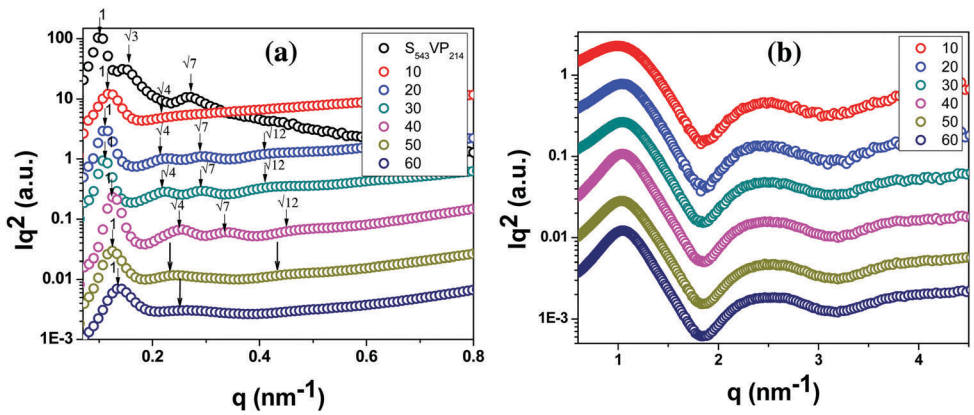

Fig. 7 SAXS intensity profiles of $S_{543}VP_{214}$/CdSe composites, at different loadings of CdSe QDs (wt%), in the (a) low-q and (b) high-q regions.

Published on 28 September 2017. Downloaded by Synchrotron Radiation Library on 05/12/2017 10:39:03.

was similar to that observed for the $S_{178}VP_{386}$/CdSe composites and represented the inter- and intra-particle scattering originating from the CdSe quantum dots present in the P4VP cylindrical domains.

The morphological information derived from the SAXS data was further corroborated using the TEM analysis of $S_{543}VP_{214}$/CdSe composites. Fig. 8 shows the TEM images obtained from the microtomed samples of $S_{543}VP_{214}$/CdSe composites.

The TEM results clearly showed the hexagonally packed cylindrical morphology of the composite samples. Moreover, the CdSe quantum dots were found to be almost exclusively located within the cylindrical domains constituted of P4VP blocks. At lower weight fractions, the CdSe quantum dots were mostly located close to the interface. As the concentration of quantum dots increased in the composites, the CdSe quantum dots were also found distributed in the interior of P4VP cylindrical domains even though the density of the particles was still much higher at the interface. Furthermore, at weight fraction $\geq$50 wt%, the morphology mostly consisted of a disordered worm-like cylindrical morphology composed of the P4VP/CdSe fraction. Hence, the TEM results corroborated the SAXS results which revealed a disordered morphology at higher weight fractions of CdSe quantum dots.

Next, the domain spacing, as ascertained from the primary peak position of the SAXS data, in the $S_{543}VP_{214}$/CdSe composites was analyzed as shown in Fig. 9. The domain spacing for the $S_{543}VP_{214}$/CdSe composites was found to display a complicated variation with the concentration of added CdSe quantum dots. The domain spacing decreased for the composite with 10 wt% quantum dots as compared to that of neat $S_{543}VP_{214}$. However, further increase in the CdSe weight fraction led to an increase in the domain spacing until w_{CdSe} = 30 wt%.

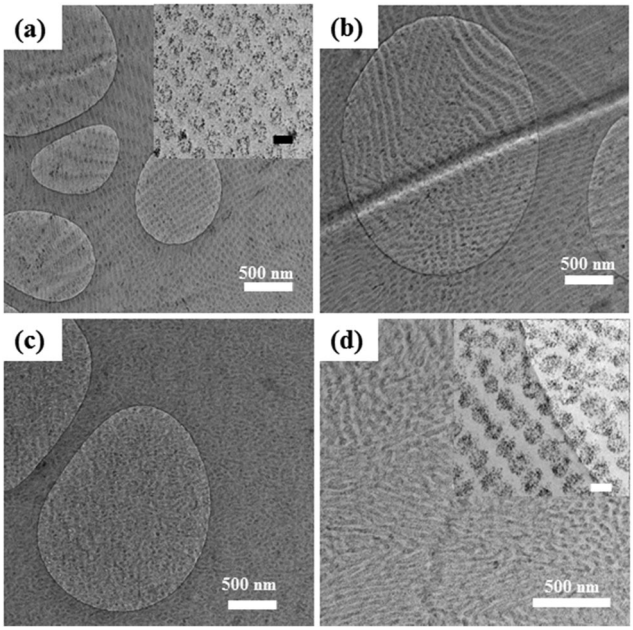

Fig. 8 TEM images of $S_{543}VP_{214}$/CdSe composites at different CdSe loadings (wt%): (a) 20, (b) 30, (c) 50, (d) 60. The inset in (a) and (d) shows a higher magnification image where the scale bar corresponds to 50 nm.

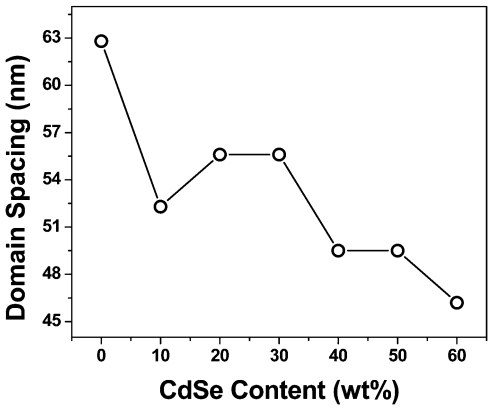

Fig. 9 Domain spacing variation with CdSe content for the $S_{543}VP_{214}$/CdSe composites.

As the weight fraction of CdSe was further increased, the domain spacing decreased again. This observation could be explained considering multiple competing factors here: the first is the domain swelling due to localization of TOPO in the PS matrix phase which will tend to increase the domain spacing, second is the interface localization of CdSe quantum dots together with the hydrophilic end of TOPO which will effectively lower the interfacial tension and will tend to decrease the interdomain spacing, and third is the increase in the interfacial area per chain due to crowding of the CdSe QDs at the interface which will tend to decrease the interdomain distance. At a lower loading of CdSe quantum dots (*ca.* 10 wt%) the reduction in the interfacial tension as well as interfacial area per chain dominates over the domain swelling, leading to decrease in the domain spacing. In this case, the PS and P4VP chains are likely to adopt a more relaxed conformation as depicted in Fig. 10. As the CdSe nanoparticle concentration increased, the domain swelling effect due to increased concentration of displaced TOPO in PS, started to dominate and, hence, led to an increase in the domain spacing. However, at much higher concentration of CdSe, plausibly the effect of increased density of CdSe quantum dots at the interface together with TOPO again dominated which consequently led to a decrease in the domain spacing. This effect of reduced interfacial tension is also evident from the disordered morphologies observed at higher weight fraction of CdSe quantum dots.

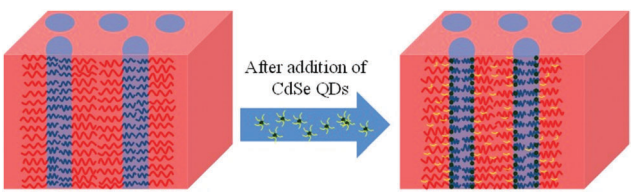

Fig. 10 Schematic illustration depicting the morphological changes, upon addition of TOPO–CdSe quantum dots, in $S_{543}VP_{214}$/CdSe composites. The localization of CdSe quantum dots together with a fraction of TOPO at the interface plausibly reduces the interfacial tension leading to a more relaxed conformation of the chains which results in the reduction of domain spacing.

This journal is © the Owner Societies 2017

Published on 28 September 2017. Downloaded by Synchrotron Radiation Library on 05/12/2017 10:39:03.

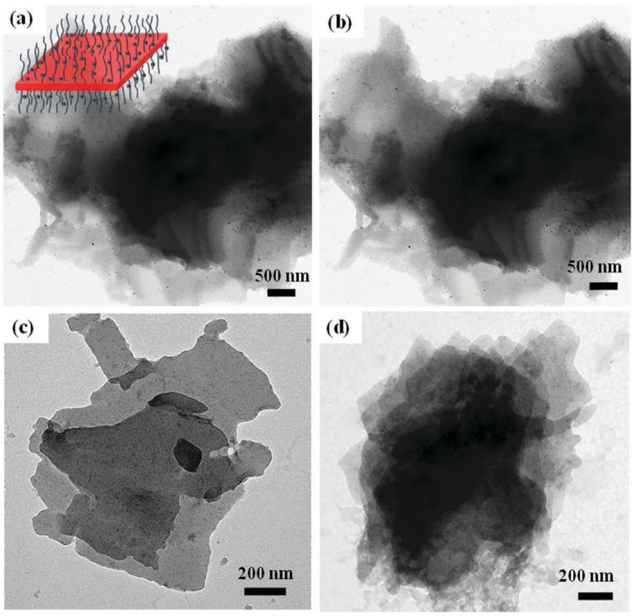

Fig. 11 TEM images of nanoobjects isolated from $S_{178}VP_{386}$/CdSe composites by swelling in methanol at different CdSe loadings (wt%): (a) 10, (b) 30, (c) 40, (d) 50.

Nano-objects from $S_{178}VP_{386}$/CdSe and $S_{543}VP_{214}$/CdSe composites

Next, we demonstrate that the self-assembled structures formed by the PS-*b*-P4VP/CdSe composites could be used to fabricate functional polymer nano-objects of well-defined shape. The approach utilized the selective swelling approach of the matrix forming block and has been described in detail elsewhere.[41] The $S_{178}VP_{386}$/CdSe composites, which had a predominately lamellae morphology at all the CdSe compositions studied were swelled in methanol so as to selectively swell the P4VP phase. The choice of methanol for selectively swelling this composite was based on the fact that neat $S_{178}VP_{386}$ displayed a morphology consisting of PS cylinders embedded in the P4VP matrix and our present experiment provided another robust proof of the existence of lamellar morphology in the composite samples. Fig. 11 shows the TEM micrographs of nano-objects isolated from the $S_{178}VP_{386}$/CdSe composites after swelling in methanol.

The figure shows the presence of nanoplate/nanosheet like structures at all the concentrations of CdSe in the composite samples. The observed polymer nanoplates clearly demonstrated the presence of lamellar morphology in these composites. These nanoplates essentially consisted of three layers where the two outer layers were composed of P4VP/CdSe blocks whereas the middle layer was composed of PS blocks. The CdSe quantum dots were clearly visible on these polymer nanosheets which demonstrated that they were strongly bound to the P4VP chains. Fig. 12(a) and (b) show the UV absorption and PL emission spectra of nanoplates obtained from $S_{178}VP_{386}$/CdSe composite samples in their methanol dispersion. The absorption spectra exhibited the characteristic absorption peaks of the CdSe quantum dots. The PL spectra also show the emission peak corresponding to the same wavelength as exhibited by the as-synthesized TOPO coated CdSe quantum dots.

The PL intensities of the nanoplates (Fig. 12(b)) were weak which could be due to the relatively poor dispersion of the nanoplates. Furthermore, it is well-known that CdSe based quantum dots exhibit lower quantum yields in polar solvents like alcoholic solvents than in non-polar solvents like chloroform and toluene.[61,62] It was also observed that the PL intensity increased and the emission peak became much sharper with increase in the weight fraction of CdSe in the nanoplates. However, the PL intensity decreased and the emission peak broadened at a much higher weight fraction of CdSe in the composites. This could be due to aggregation of quantum dots leading to quenching of the PL emission.

Fig. 13 shows the TEM micrographs of nano-objects isolated from the $S_{543}VP_{214}$/CdSe composites after swelling in cyclohexane. The figure clearly showed the presence of well dispersed polymer nanofibers until 30 wt% CdSe loading.

This was expected since the $S_{543}VP_{214}$/CdSe composites exhibited cylindrical morphology of P4VP/CdSe blocks dispersed in the PS matrix. Hence, these nanofibres consisted of a P4VP/CdSe cylindrical core which was insoluble in cyclohexane and a hairy

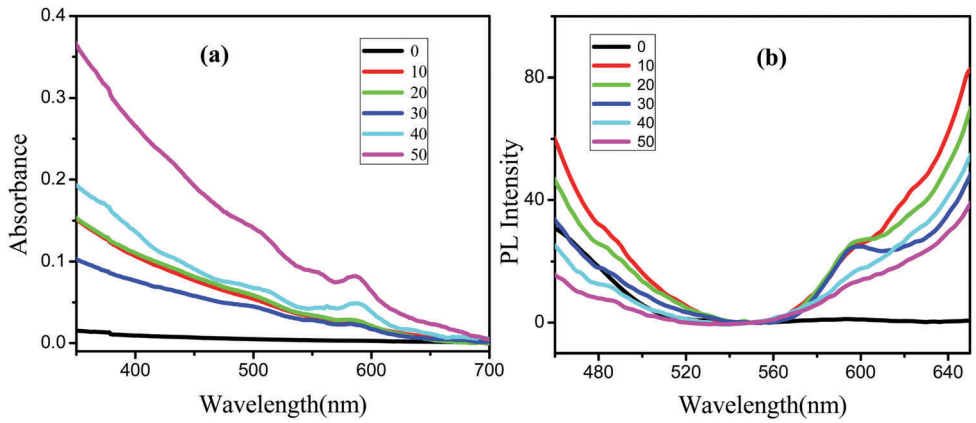

Fig. 12 (a) UV-vis and (b) PL spectra of the dispersion of nanoobjects, isolated from $S_{178}VP_{386}$/CdSe composites, in methanol.

Published on 28 September 2017. Downloaded by Synchrotron Radiation Library on 05/12/2017 10:39:03.

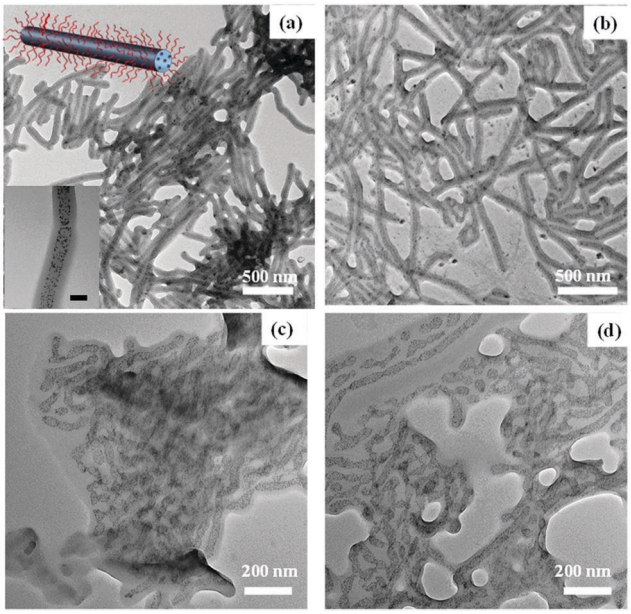

Fig. 13 TEM images of nanoobjects isolated from $S_{543}VP_{214}$/CdSe composites by swelling in cyclohexane at different CdSe loadings (wt%): (a) 20, (b) 30, (c) 50, (d) 60. The inset in (a) shows the higher magnification image where the scale bar corresponds to 50 nm. The CdSe QDs could be clearly seen localized in the nano-objects.

shell of PS chains, which though soluble in cyclohexane were retained on the nanofibre because of their covalent linkage with the P4VP blocks. The presence of CdSe in the nanofibers also provided further strong evidence that these quantum dots were bound to P4VP blocks. Furthermore, at a higher concentration of quantum dots in the $S_{543}VP_{214}$/CdSe composites, the nano-objects mostly consisted of a mixture of short nanofibers and nanospheres. This was expected since, as discussed before, at $w_{CdSe} > 40$ wt%, the $S_{543}VP_{214}$/CdSe composites exhibited a disordered worm-like morphology.

Fig. 14 shows the UV absorption and PL emission spectra of nanofibers obtained from $S_{543}VP_{214}$/CdSe composite samples in their cyclohexane dispersion.

The absorption spectra were similar to those observed for nano-objects from the $S_{178}VP_{386}$/CdSe composite and exhibited the characteristic absorption peaks of the CdSe quantum dots. The emission peak in the PL spectra, however, was much more intense for the nanofibers obtained here. This could be attributed to the fact that the CdSe containing nanofibers were present in a non-polar solvent. Furthermore, the intensity of the PL emission peak increased with increase in the CdSe concentration in the composite samples. In this case, the CdSe quantum dots at higher concentration were more uniformly distributed through the P4VP cylindrical domains unlike in $S_{178}VP_{386}$/CdSe composite samples where the quantum dots were mostly aggregated at the interface. The isolated nano-objects containing CdSe quantum dots may have potential applications in fluorescence labeling, chemical sensing, light emitting devices and many others.

Conclusions

The self-assembly of the cylinder-forming PS-*b*-P4VP BCP mixed with TOPO capped CdSe QDs was investigated. It was demonstrated that the QDs were enthalpically compatible with the P4VP chains, driven *via* ligand-displacement of the TOPO from the QD surface. However, the QDs were found to localize preferentially at the PS/P4VP interphase plausibly to gain translational entropy. Most interestingly, the morphological transformation observed with increasing weight fraction of the QDs in the BCP/QD composite was found to be driven by the migration of the displaced TOPO from the QD surface to the PS phase such that its effective volume fraction increased. Hence, the PS-*b*-P4VP BCP with PS as the minority block exhibited morphological transformation from cylindrical to lamellar morphology in its composite with QDs. Furthermore, the preferred localization of the QDs at the interface led to the formation of a novel trilayer lamellar morphology where the middle layer was mostly composed of CdSe QDs. The trilayer morphology was also evident from the suppression of the primary scattering peak, relative to higher order peaks, in the SAXS data of these samples. The morphological transformation was accompanied by a significant increase in the domain spacing due to excessive stretching of the longer P4VP chains so as to minimize the interfacial energy. However, in the

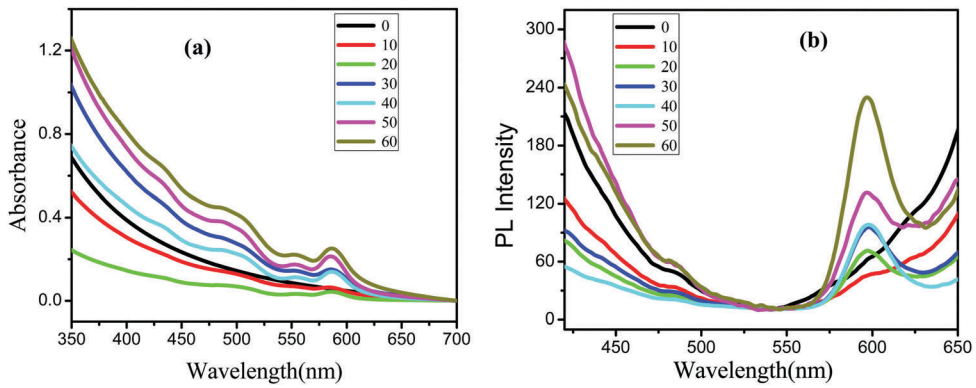

Fig. 14 (a) UV-vis and (b) PL spectra of the dispersion of nanoobjects, isolated from $S_{543}VP_{214}$/CdSe composites, in cyclohexane.

 This journal is © the Owner Societies 2017

Published on 28 September 2017. Downloaded by Synchrotron Radiation Library on 05/12/2017 10:39:03.

PS-*b*-P4VP/CdSe composites with P4VP as the minority block, cylindrical morphology was retained and the domain spacing essentially decreased due to dominance of the co-surfactant effect due to localization of CdSe and the plausible presence of a fraction of TOPO at the interface. It was further demonstrated that these PS-*b*-P4VP/CdSe self-assembled hybrid materials could be used to obtain isolated photoluminescent core–shell nanoobjects, such as nanoplates and nanofibers. Such photoluminescent polymer nanoobjects could have potential applications in biological targeting and fluorescence labeling.

Conflicts of interest

There are no conflicts to declare.

Acknowledgements

This research was supported by a grant from the Department of Science and Technology, India (SR/NM/NS-1439/2014), Deutsche Forschungsgemeinschaft, Germany (STA 324/51-1) and in part from the Ministry of Science and Technology, Taiwan (MOST 104-2633-M-007-001 for H.-L. Chen). SS is thankful to the Council of Scientific and Industrial Research (CSIR) for a Junior Research Fellowship. We also acknowledge the help extended by Prof. Sameer Sapra at IIT Delhi for the UV and PL measurements.

References

1 I. W. Hamley, *The physics of block copolymers*, Oxford University Press, Oxford, New York, 1998.
2 L. Leibler, Theory of Microphase Separation in Block Copolymers, *Macromolecules*, 1980, **13**, 1602–1617.
3 M. R. Bockstaller, R. A. Mickiewicz and E. L. Thomas, Block Copolymer Nanocomposites: Perspectives for Tailored Functional Materials, *Adv. Mater.*, 2005, **17**, 1331–1349.
4 A. Haryono and W. H. Binder, Controlled Arrangement of Nanoparticle Arrays in Block-Copolymer Domains, *Small*, 2006, **2**, 600–611.
5 M. Grzelczak, J. Vermant, E. M. Furst and L. M. Liz-Marzán, Directed Self-Assembly of Nanoparticles, *ACS Nano*, 2010, **4**, 3591–3605.
6 J. Kao, K. Thorkelsson, P. Bai, B. J. Rancatore and T. Xu, Toward functional nanocomposites: taking the best of nanoparticles, polymers, and small molecules, *Chem. Soc. Rev.*, 2013, **42**, 2654–2678.
7 Y. Lin, A. Böker, J. He, K. Sill, H. Xiang, C. Abetz, X. Li, J. Wang, T. Emrick, S. Long, Q. Wang, A. Balazs and T. P. Russell, Self-directed self-assembly of nanoparticle/copolymer mixtures, *Nature*, 2005, **434**, 55–59.
8 A. C. Balazs, T. Emrick and T. P. Russell, Nanoparticle Polymer Composites: Where Two Small Worlds Meet, *Science*, 2006, **314**, 1107–1110.
9 J. J. Chiu, B. J. Kim, E. J. Kramer and D. J. Pine, Control of Nanoparticle Location in Block Copolymers, *J. Am. Chem. Soc.*, 2005, **127**, 5036–5037.
10 A. Horechyy, N. E. Zafeiropoulos, B. Nandan, P. Formanek, F. Simon, A. Kiriy and M. Stamm, Highly ordered arrays of magnetic nanoparticles prepared via block copolymer assembly, *J. Mater. Chem.*, 2010, **20**, 7734.
11 J. Kao, P. Bai, J. M. Lucas, A. P. Alivisatos and T. Xu, Size-Dependent Assemblies of Nanoparticle Mixtures in Thin Films, *J. Am. Chem. Soc.*, 2013, **135**, 1680–1683.
12 B. Sarkar and P. Alexandridis, Block copolymer–nanoparticle composites: structure, functional properties, and processing, *Prog. Polym. Sci.*, 2015, **40**, 33–62.
13 B. Sarkar and P. Alexandridis, Self-Assembled Block Copolymer–Nanoparticle Hybrids: Interplay between Enthalpy and Entropy, *Langmuir*, 2012, **28**, 15975–15986.
14 R. B. Thompson, V. V. Ginzburg, M. W. Matsen and A. C. Balazs, Block Copolymer-Directed Assembly of Nanoparticles: Forming Mesoscopically Ordered Hybrid Materials, *Macromolecules*, 2002, **35**, 1060–1071.
15 J. Huh, V. V. Ginzburg and A. C. Balazs, Thermodynamic Behavior of Particle/Diblock Copolymer Mixtures: Simulation and Theory, *Macromolecules*, 2000, **33**, 8085–8096.
16 R. B. Thompson, Predicting the Mesophases of Copolymer-Nanoparticle Composites, *Science*, 2001, **292**, 2469–2472.
17 J.-Y. Lee, R. B. Thompson, D. Jasnow and A. C. Balazs, Entropically Driven Formation of Hierarchically Ordered Nanocomposites, *Phys. Rev. Lett.*, 2002, **89**, 155503.
18 J. Y. Lee, R. B. Thompson, D. Jasnow and A. C. Balazs, Effect of Nanoscopic Particles on the Mesophase Structure of Diblock Copolymers, *Macromolecules*, 2002, **35**, 4855–4858.
19 G. A. Buxton, J. Y. Lee and A. C. Balazs, Computer Simulation of Morphologies and Optical Properties of Filled Diblock Copolymers, *Macromolecules*, 2016, **36**, 9631–9637.
20 A. I. Chervanyov and A. C. Balazs, Effect of particle size and shape on the order–disorder phase transition in diblock copolymers, *J. Chem. Phys.*, 2003, **119**, 3529–3534.
21 J. Y. Lee, R. B. Thompson, D. Jasnow and A. C. Balazs, Self-assembly of a binary mixture of particles and diblock copolymers, *Faraday Discuss.*, 2003, **123**, 121–131.
22 J. Y. Lee, Z. Shou and A. C. Balazs, Predicting the Morphologies of Confined Copolymer/Nanoparticle Mixtures, *Macromolecules*, 2003, **36**, 7730–7739.
23 M. R. Bockstaller, Y. Lapetnikov, S. Margel and E. L. Thomas, Size-Selective Organization of Enthalpic Compatibilized Nanocrystals in Ternary Block Copolymer/Particle Mixtures, *J. Am. Chem. Soc.*, 2003, **125**, 5276–5277.
24 J. J. Chiu, B. J. Kim, G.-R. Yi, J. Bang, E. J. Kramer and D. J. Pine, Distribution of Nanoparticles in Lamellar Domains of Block Copolymers, *Macromolecules*, 2007, **40**, 3361–3365.
25 B. J. Kim, J. Bang, C. J. Hawker, J. J. Chiu, D. J. Pine, S. G. Jang, S.-M. Yang and E. J. Kramer, Creating Surfactant Nanoparticles for Block Copolymer Composites through Surface Chemistry, *Langmuir*, 2007, **23**, 12693–12703.
26 B. J. Kim, J. Bang, C. J. Hawker and E. J. Kramer, Effect of Areal Chain Density on the Location of Polymer-Modified

Published on 28 September 2017. Downloaded by Synchrotron Radiation Library on 05/12/2017 10:39:03.

Gold Nanoparticles in a Block Copolymer Template, *Macromolecules*, 2006, **39**, 4108–4114.

27 B. J. Kim, G. H. Fredrickson and E. J. Kramer, Effect of Polymer Ligand Molecular Weight on Polymer-Coated Nanoparticle Location in Block Copolymers, *Macromolecules*, 2008, **41**, 436–447.

28 B. J. Kim, G. H. Fredrickson, J. Bang, C. J. Hawker and E. J. Kramer, Tailoring Core–Shell Polymer-Coated Nanoparticles as Block Copolymer Surfactants, *Macromolecules*, 2009, **42**, 6193–6201.

29 B. J. Kim, J. J. Chiu, G.-R. Yi, D. J. Pine and E. J. Kramer, Nanoparticle-Induced Phase Transitions in Diblock-Copolymer Films, *Adv. Mater.*, 2005, **17**, 2618–2622.

30 S.-W. Yeh, T.-L. Wu, K.-H. Wei, Y.-S. Sun and K. S. Liang, Effect of incorporated CdS nanoparticles on the crystallinity and morphology of poly(styrene-*b*-ethylene oxide) diblock copolymers, *J. Polym. Sci., Part B: Polym. Phys.*, 2005, **43**, 1220–1229.

31 S.-W. Yeh, K.-H. Wei, Y.-S. Sun, U.-S. Jeng and K. S. Liang, CdS Nanoparticles Induce a Morphological Transformation of Poly(styrene-*b*-4-vinylpyridine) from Hexagonally Packed Cylinders to a Lamellar Structure, *Macromolecules*, 2005, **38**, 6559–6565.

32 Z. Li, H. Sai, S. C. Warren, M. Kamperman, H. Arora, S. M. Gruner and U. Wiesner, Metal Nanoparticle–Block Copolymer Composite Assembly and Disassembly, *Chem. Mater.*, 2009, **21**, 5578–5584.

33 S. G. Jang, B. J. Kim, C. J. Hawker and E. J. Kramer, Bicontinuous Block Copolymer Morphologies Produced by Interfacially Active, Thermally Stable Nanoparticles, *Macromolecules*, 2011, **44**, 9366–9373.

34 C.-T. Lo, B. Lee, V. G. Pol, N. L. Dietz Rago, S. Seifert, R. E. Winans and P. Thiyagarajan, Effect of Molecular Properties of Block Copolymers and Nanoparticles on the Morphology of Self-Assembled Bulk Nanocomposites, *Macromolecules*, 2007, **40**, 8302–8310.

35 L. Yao, Y. Lin and J. J. Watkins, Ultrahigh Loading of Nanoparticles into Ordered Block Copolymer Composites, *Macromolecules*, 2014, **47**, 1844–1849.

36 Y. Gai, Y. Lin, D.-P. Song, B. M. Yavitt and J. J. Watkins, Strong Ligand–Block Copolymer Interactions for Incorporation of Relatively Large Nanoparticles in Ordered Composites, *Macromolecules*, 2016, **49**, 3352–3360.

37 B. Nandan and A. Horechyy, Hairy Core–Shell Polymer Nano-objects from Self-Assembled Block Copolymer Structures, *ACS Appl. Mater. Interfaces*, 2015, **7**, 12539–12558.

38 W. Li, S. Liu, R. Deng and J. Zhu, Encapsulation of Nanoparticles in Block Copolymer Micellar Aggregates by Directed Supramolecular Assembly, *Angew. Chem., Int. Ed.*, 2011, **50**, 5865–5868.

39 R. Liang, J. Xu, W. Li, Y. Liao, K. Wang, J. You, J. Zhu and W. Jiang, Precise Localization of Inorganic Nanoparticles in Block Copolymer Micellar Aggregates: From Center to Interface, *Macromolecules*, 2015, **48**, 256–263.

40 J. Wang, W. Li and J. Zhu, Encapsulation of inorganic nanoparticles into block copolymer micellar aggregates: strategies and precise localization of nanoparticles, *Polymer*, 2014, **55**, 1079–1096.

41 J. Pal, S. Sanwaria, R. Srivastava, B. Nandan, A. Horechyy, M. Stamm and H.-L. Chen, Hairy polymer nanofibers via self-assembly of block copolymers, *J. Mater. Chem.*, 2012, **22**, 25102.

42 S. Sanwaria, S. Singh, A. Horechyy, P. Formanek, M. Stamm, R. Srivastava and B. Nandan, Multifunctional core–shell polymer–inorganic hybrid nanofibers prepared via block copolymer self-assembly, *RSC Adv.*, 2015, **5**, 89861–89868.

43 S. Sanwaria, A. Horechyy, D. Wolf, C.-Y. Chu, H.-L. Chen, P. Formanek, M. Stamm, R. Srivastava and B. Nandan, Helical Packing of Nanoparticles Confined in Cylindrical Domains of a Self-Assembled Block Copolymer Structure, *Angew. Chem., Int. Ed.*, 2014, **53**, 9090–9093.

44 U. Soni, A. Pal, S. Singh, M. Mittal, S. Yadav, R. Elangovan and S. Sapra, Simultaneous Type-I/Type-II Emission from CdSe/CdS/ZnSe Nano-Heterostructures, *ACS Nano*, 2014, **8**, 113–123.

45 U.-S. Jeng, C. H. Su, C.-J. Su, K.-F. Liao, W.-T. Chuang, Y.-H. Lai, J.-W. Chang, Y.-J. Chen, Y.-S. Huang, M.-T. Lee, K.-L. Yu, J.-M. Lin, D.-G. Liu, C.-F. Chang, C.-Y. Liu, C.-H. Chang and K. S. Liang, A small/wide-angle X-ray scattering instrument for structural characterization of air–liquid interfaces, thin films and bulk specimens, *J. Appl. Crystallogr.*, 2010, **43**, 110–121.

46 M. Wang, S. Kumar, A. Lee, N. Felorzabihi, L. Shen, F. Zhao, P. Froimowicz, G. D. Scholes and M. A. Winnik, Nanoscale Co-organization of Quantum Dots and Conjugated Polymers Using Polymeric Micelles As Templates, *J. Am. Chem. Soc.*, 2008, **130**, 9481–9491.

47 X.-S. Wang, T. E. Dykstra, M. R. Salvador, I. Manners, G. D. Scholes and M. A. Winnik, Surface Passivation of Luminescent Colloidal Quantum Dots with Poly(Dimethylaminoethyl methacrylate) through a Ligand Exchange Process, *J. Am. Chem. Soc.*, 2004, **126**, 7784–7785.

48 M. Kuno, J. K. Lee, B. O. Dabbousi, F. V. Mikulec and M. G. Bawendi, The band edge luminescence of surface modified CdSe nanocrystallites: probing the luminescing state, *J. Chem. Phys.*, 1997, **106**, 9869.

49 H. Skaff and T. Emrick, The use of 4-substituted pyridines to afford amphiphilic, pegylated cadmium selenide nanoparticles, *Chem. Commun.*, 2003, 52–53, ESI:† TEM images and absorbance profiles. See http://www.rsc.org/suppdata/cc/b2/b208718a/.

50 M. Wang, J. K. Oh, T. E. Dykstra, X. Lou, G. D. Scholes and M. A. Winnik, Surface Modification of CdSe and CdSe/ZnS Semiconductor Nanocrystals with Poly(*N*,*N*-dimethylaminoethyl methacrylate), *Macromolecules*, 2006, **39**, 3664–3672.

51 S. Zou, R. Hong, T. Emrick and G. C. Walker, Ordered CdSe Nanoparticles within Self-Assembled Block Copolymer Domains on Surfaces, *Langmuir*, 2007, **23**, 1612–1614.

52 S. Ludwigs, A. Böker, V. Abetz, A. H. E. Müller and G. Krausch, Phase behavior of linear polystyrene-*block*-poly(2-vinylpyridine)-*block*-poly(*tert*-butyl methacrylate) triblock terpolymers, *Polymer*, 2003, **44**, 6815–6823.

 This journal is © the Owner Societies 2017

Published on 28 September 2017. Downloaded by Synchrotron Radiation Library on 05/12/2017 10:39:03.

53 G. Gobius du Sart, I. Vukovic, G. Alberda van Ekenstein, E. Polushkin, K. Loos and G. ten Brinke, Self-Assembly of Supramolecular Triblock Copolymer Complexes, *Macromolecules*, 2010, **43**, 2970–2980.

54 C.-J. Chang, Y.-H. Lee, H.-L. Chen, C.-H. Chiang, H.-F. Hsu, C.-C. Ho, W.-F. Su and C.-A. Dai, Effect of rod–rod interaction on self-assembly behavior of ABC π-conjugated rod–coil–coil triblock copolymers, *Soft Matter*, 2011, **7**, 10951.

55 C. Lai, W. B. Russel and R. A. Register, Scaling of Domain Spacing in Concentrated Solutions of Block Copolymers in Selective Solvents, *Macromolecules*, 2002, **35**, 4044–4049.

56 J. J. Watkins, G. D. Brown, V. S. RamachandraRao, M. A. Pollard and T. P. Russell, Phase Separation in Polymer Blends and Diblock Copolymers Induced by Compressible Solvents, *Macromolecules*, 1999, **32**, 7737–7740.

57 S.-C. Chen, S.-W. Kuo, U.-S. Jeng, C.-J. Su and F.-C. Chang, On Modulating the Phase Behavior of Block Copolymer/Homopolymer Blends via Hydrogen Bonding, *Macromolecules*, 2010, **43**, 1083–1092.

58 T. Hashimoto, H. Tanaka and H. Hasegawa, Ordered structure in mixtures of a block copolymer and homopolymers. 2. Effects of molecular weights of homopolymers, *Macromolecules*, 1990, **23**, 4378–4386.

59 H. Tanaka, H. Hasegawa and T. Hashimoto, Ordered structure in mixtures of a block copolymer and homopolymers. 1. Solubilization of low molecular weight homopolymers, *Macromolecules*, 1991, **24**, 240–251.

60 E. Kim, H. Ahn, D. Y. Ryu, W. Joo, J. K. Kim, J. Jung and T. Chang, Closed-Loop Transition Induced by Homopolymers, *Macromolecules*, 2008, **41**, 9875–9881.

61 M. Wang, M. Zhang, J. Qian, F. Zhao, L. Shen, G. D. Scholes and M. A. Winnik, Enhancing the Photoluminescence of Polymer-Stabilized CdSe/CdS/ZnS Core/Shell/Shell and CdSe/ZnS Core/Shell Quantum Dots in Water through a Chemical-Activation Approach, *Langmuir*, 2009, **25**, 11732–11740.

62 M. Zhang, L. Rene-Boisneuf, Y. Hu, K. Moozeh, Y. Hassan, G. Scholes and M. A. Winnik, Preparation and photo/chemical-activation of wormlike network micelles of core–shell quantum dots and block copolymer hybrids, *J. Mater. Chem.*, 2011, **21**, 9692.